Local correlated motions in aqueous solution of sodium chloride

Yuya Shinohara,[1,2,*] Wojciech Dmowski,[2,3] Takuya Iwashita,[4] Daisuke Ishikawa,[5] Alfred Q. R. Baron,[6] and Takeshi Egami[2,3,7,†]

[1]*Materials Science and Technology Division, Oak Ridge National Laboratory, Oak Ridge, Tennessee 37831, USA*
[2]*Shull Wollan Center, University of Tennessee, Knoxville and Oak Ridge National Laboratory, Oak Ridge, Tennessee 37831, USA*
[3]*Department of Materials Science and Engineering, University of Tennessee, Knoxville, Tennessee 37996, USA*
[4]*Department of Integrated Science and Technology, Oita University, Dannoharu, Oita 870-1192, Japan*
[5]*Research and Utilization Division, Japan Synchrotron Radiation Research Institute (JASRI), Sayo, Hyogo 679-5198, Japan*
[6]*Materials Dynamics Laboratory, RIKEN SPring-8 Center, RIKEN, Sayo, Hyogo 679-5148, Japan*
[7]*Department of Physics and Astronomy, University of Tennessee, Knoxville, Tennessee 37996, USA*

(Received 9 March 2019; published 17 June 2019)

Real-space motions of molecules and ions in an aqueous solution of sodium chloride are studied with high-resolution inelastic x-ray scattering. We focus on the correlated dynamics of water molecules and salt ions, instead of the instantaneous structure and the rotational and reorientation dynamics that have been studied using scattering techniques and optical spectroscopy, respectively. The real-space analysis in terms of the Van Hove function illustrates the effect of salt ions to slow down the local correlated dynamics of surrounding water in the hydration shells.

DOI: 10.1103/PhysRevMaterials.3.065604

I. INTRODUCTION

Aqueous solutions of salt and electrolyte solutions are ubiquitous and of fundamental importance in many applications and in science, including the life sciences. The hydration shells of biomolecules strongly influence their structure and properties [1], whereas the physical properties of electrolyte solutions are key to achieving high performance in batteries. In addition, 97.5% of water on Earth is salt water [2]. Many studies have been conducted to understand the mechanism of changes in various properties with the addition of salt. For example, the addition of salt to water induces a change in viscosity in an ion-specific manner and shows both increases and decreases upon the addition. A semiempirical description of this behavior is given by the Jones-Dole equation [3,4], in which the so-called B coefficient represents the linear increase and decrease in viscosity with concentration, but its understanding lacks a microscopic and molecular picture. Despite significant experimental and theoretical efforts [5–18], a molecular-level understanding of salt water, particularly its transport properties, is elusive and remains controversial [19]. Conventional neutron/x-ray scattering makes it possible to obtain an instantaneous (snapshot) structure of water molecules in salt solution [5,13,20–24], while optical spectroscopy provides us with translational, rotational, and reorientation dynamics of water molecules [6–11,25–28]. Molecular dynamics (MD) simulation have played a major role regarding visualizing molecular motions in a salt solution to complement the experimental observations [29–31]. However, water models are still far from perfect and sometimes fail to reproduce experimental results even qualitatively [32,33]. Indeed, the current theory and molecular dynamics simulation cannot predict the values of viscosity even qualitatively nor explain the mechanism of the decrease in the viscosity. Recent spectroscopy studies found the correlation between B coefficients and various experimental quantities [7,8] and a coarse-grained model of electrolyte solutions successfully reproduces the basic trend of transport properties [17,34]; still, a molecular-level understanding of this phenomenon has been elusive.

One of the issues is an incomplete understanding of the collective motions of molecules, which are directly relevant to the transport properties of liquid. So far, the difficulty for obtaining the molecular-level understanding lies in identifying the collective molecular motions of water experimentally, in a timescale relating to the forming/breaking of a hydrogen bond around picoseconds. We have previously identified that the local collective motions of molecules play a vital role in determining the viscosity in liquid. At high temperatures, the time required for an atom losing or gaining one neighbor is a critical quantity that determines the viscosity of the liquid [35]. This local configurational excitation time was found to be almost equal to the Maxwell relaxation time, τ_M, for simple metallic liquids [35] and pure water [36,37] at temperatures above a crossover temperature, T_A, which defines the crossover from the Arrhenius behavior to the non-Arrhenius behavior [38]. Here, $\tau_M = \eta/G_\infty$ determines the timescale of viscous phenomena, where η is viscosity and G_∞ is instantaneous shear modulus. The fact that the equality holds for these entirely different properties, i.e., one macroscopic (τ_M) and the other microscopic (τ_{LC}), of liquids suggests that this is universal and the process of losing/gaining one neighbor is an elementary excitation in liquids [39].

To shed light on the collective and correlated motions of molecules by experiment, we have employed a different technique: analysis of liquid dynamics using the Van Hove

*shinoharay@ornl.gov
†egami@utk.edu

function [40]. The molecular Van Hove function, $G(R,t)$, is defined as

$$G(R,t) = \frac{1}{4\pi\rho NR^2}\sum_{i,j}\delta(R - |\boldsymbol{r}_i(0) - \boldsymbol{r}_j(t)|), \qquad (1)$$

where ρ is the average number density of molecules, N is the number of molecules in the system, and $\boldsymbol{r}_i(t)$ is the position of the ith molecule at time t. The Van Hove function represents the probability for a molecule at the origin $R = 0$ at time $t = 0$ finding another molecule at distance R, at time t, and is regarded as the time-dependent pair-distribution function (PDF). Thus, the real-space molecular correlated motions can be visualized using the Van Hove function. Previously, it was difficult to obtain the Van Hove function experimentally because it requires us to obtain inelastic x-ray/neutron scattering data over wide ranges of energy (E) and momentum transfer (Q) with a high-E and -Q resolution. Recent progress in high-resolution inelastic x-ray scattering (IXS) using highly brilliant synchrotron radiation makes it possible to obtain IXS spectra over sufficiently wide ranges of E and Q so that $G(R,t)$ can be calculated via the double Fourier transformation of the IXS spectra over E and Q [41,42]. This technique has shown the detailed correlated motions of molecules in a picosecond timescale and its close relationship with macroscopic viscosity in pure water [36,37] as well as those of simple metallic liquids [43,44].

In this paper, we employ this technique to study NaCl aqueous solutions with the aim of examining the effect of Na^+ and Cl^- ions on the dynamics of water molecules in real space. The Van Hove functions are successfully obtained and show the correlated motions of water molecules and ions; the slowing down of correlated dynamics upon the addition of NaCl is observed. Furthermore, the detailed analysis provides the information about the interaction between a water molecule and ions. This research paves the way for elucidating the molecular-level mechanism of water dynamics in the presence of various salts.

II. MATERIALS AND METHODS

A. Materials and inelastic and elastic x-ray scattering of salt water

Sodium chloride (Fisher Scientific) was used as received. Salt solutions were prepared in approximately 30 cm^3 of fresh deionized water, shaken by hand, and were allowed to sit overnight before experiments. The molality of a solution, m, was calculated to be 0.75, 1.5, 2.26, and 3.0 mol/kg.

Inelastic x-ray scattering measurements were carried out at the RIKEN Quantum NanoDynamics Beamline (BL43LXU) [45], SPring-8, in Hyogo, Japan. Salt-solution samples were placed between two single-crystal-diamond windows (thickness 0.3 mm) and the thickness of the sample was 3.0 mm (m = 0, 0.75, 1.5, 2.26 mol/kg) or 1.0 mm (m = 3.0 mol/kg). The temperature of the sample was kept at 303 K. The energy of the incident x-ray was 21.747 keV and the IXS spectra were collected over a wide Q-E range ($0.94 < Q < 10.1$ Å^{-1}, $-10 < E < 100$ meV for the samples of m = 0, 0.75, 1.5, and 2.26 mol/kg, and $-10 < E < 70$ meV for the sample of m = 3.0 mol/kg). The Q resolution was 0.4–1 Å^{-1}. To estimate the energy resolution, the IXS spectra were measured for borosilicate glass of 3 mm thick.

To normalize the IXS spectra, the scattering intensity profiles of the salt-water solution, $I(Q)$, were separately measured at the 6ID-D beam line, APS (Argonne National Laboratory, USA). The data were taken with a 100.241 keV x-ray with an amorphous silicon flat-panel detector (XRD 1621, Perkin-Elmer, Inc.), and the sample-to-detector distance was 395 mm. Two-dimensional high-energy x-ray diffraction patterns were converted into one-dimensional scattering intensity profiles using FIT2D [46]. After completing the conventional correction procedure such as absorption correction and subtracting Compton scattering [47], the profiles of the absolute scattering intensity were used for normalizing the IXS data.

B. Calculation of the Van Hove function from IXS data

The measured IXS data, $I_{\mathrm{raw}}(Q,E)$, were reduced to the Van Hove function, $G(R,t)$, by the double Fourier transformation over momentum transfer Q and energy transfer E, following the procedures discussed in the previous studies [36,37]. In the analysis of pure water, we used a molecular form factor, $f_{H_2O}(Q)$, as in the previous studies to obtain the structure factor, $S(Q,E)$, and thereby the molecular Van Hove function, $G(R,t)$, from the scattering intensity $I(Q,E)$: $S(Q,E) = I(Q,E)/\langle f_{H_2O}(Q)\rangle^2$. In the analysis of salt water, we divided $I(Q,E)$ by the square of the averaged molecular form factor, $\langle f(Q)\rangle^2$, defined as follows:

$$\langle f(Q)\rangle = c_{H_2O}\langle f_{H_2O}(Q)\rangle + c_{Na^+}\langle f_{Na^+}(Q)\rangle + c_{Cl^-}\langle f_{Cl^-}(Q)\rangle, \qquad (2)$$

where c_i is the atomic concentration of species i whose Q-dependent x-ray molecular/ionic form factor is $f_i(Q)$, and the angular bracket represents the azimuthal averaging. Here we assumed a simple ionic picture in which the ions are fully dissolved in water and the form factor of each ion is calculated using a free-ion approximation [48]. The molecular form factor of water is taken from Ref. [49]. After that, the Van Hove function is calculated by the double Fourier transformation of $S(Q,E)$. As a result, $S(Q,E)$ and $G(R,t)$ represent the total spatiotemporal correlation among water molecules, cations, and anions, the detailed description of which is discussed in the following section.

The effect of energy resolution is removed in the time domain, instead of the energy domain as in the conventional IXS studies. The IXS spectra of borosilicate glass of 3 mm thick were used as the energy-resolution function, $M(Q,E)$. We then calculated its Fourier transform over E, $m(Q,t)$, for which Q is at the first peak of the scattering function. The decaying behavior of the resolution function was fitted by using the summation of a Gaussian function and an exponential function, as expected from a pseudo-Voigt approximation of the energy-resolution function in the energy domain: $m(Q,t) = m_1\exp(-t^2/\tau_G^2) + m_2\exp(-t/\tau_E)$. The fitting results showed that $\tau_G = 0.17$ ps and $\tau_E = 3$ ps with $m_1 = 0.09$ and $m_2 = 0.91$. Assuming $m(Q,t)$ is not highly dependent on Q, the effect of the energy-resolution function is reasonably removed by dividing the intermediate scattering function,

TABLE I. List of the averaged weight factor.

Molality (mol/kg)	0.75	1.5	2.26	3.0
Water-Water	0.894	0.804	0.728	0.663
Water-Na	0.038	0.068	0.092	0.111
Water-Cl	0.065	0.116	0.157	0.189

$F(Q,t)$, by $m(Q,t)$. The validity of the assumption will be addressed in a separate study.

C. Partial Van Hove function

In PDF analysis of a multicomponent system, several kinds of structure factors and corresponding PDFs have been proposed. Here we introduce a partial dynamic structure factor and the partial Van Hove function following the Faber-Ziman formalism of a partial structure factor. The partial Van Hove function between the α and the β, $G_{\alpha\beta}(R,t)$, is defined as

$$G_{\alpha\beta}(R,t) = \frac{V}{4\pi N_\alpha N_\beta R^2} \sum_{i\in\{\alpha\}} \sum_{j\in\{\beta\}} \delta(R - |r_i(0) - r_j(t)|), \quad (3)$$

where $\{\alpha\}$ represent the atoms (or molecules or ions) of α species. Here, V is the volume and N_α and N_β are the number of molecules of the α and β species, respectively. With this definition, $G_{\alpha\beta}(R,t) \to 1$ with $R \to \infty$ and the total Van Hove function is given by $G_{\rm tot}(R,t) = \sum_{\alpha\beta} N_\alpha N_\beta G_{\alpha\beta}(R,t) / \sum_\alpha N_\alpha$. Equivalently, we can define the dynamic structure factor, $S_{\alpha\beta}(Q,E)$, as the Fourier transform of the partial Van Hove function, $S_{\alpha\beta} = \mathcal{F}(G_{\alpha\beta})$, such that $S_{\alpha\beta}(Q,E) \to 1$ with $Q \to \infty$, and

$$\sum_{\alpha,\beta} w_{\alpha\beta}(Q) S_{\alpha\beta}(Q,E) = S(Q,E). \quad (4)$$

Here, the weighting factor $w_{\alpha\beta}(Q)$ is given by the products of concentration c_i and form factor $f_i(Q)$ of the ith species:

$$w_{\alpha\beta}(Q) = \frac{c_\alpha c_\beta f_\alpha(Q) f_\beta(Q)}{\left[\sum_\alpha c_\alpha f_\alpha(Q)\right]^2}. \quad (5)$$

Figure 1 shows $w_{\alpha\beta}(Q)$ for the aqueous-solution samples used in this study. Because of the Q dependence of $w_{\alpha\beta}(Q)$, the calculation of the partial Van Hove function from the experimental results is not straightforward. Meanwhile, our measurement at a single-incident x-ray energy does not allow us to separate each individual contribution $S_{\alpha\beta}(Q,E)$ from the measured dynamic structure factor. Also, the Q dependence of $w_{\alpha\beta}(Q)$ is much smaller compared to that of the form factor $f_\alpha(Q)$, as shown in Fig. 1. Therefore, we employ the approximation of weight factors proposed by Warren and introduce the averaged weight factor defined by

$$\overline{w_{\alpha\beta}} = \frac{1}{Q_{\rm max}} \int_0^{Q_{\rm max}} w_{\alpha\beta}(Q) dQ. \quad (6)$$

Here, we used $Q_{\rm max} = 10.0$ Å^{-1} and the results for Water-Water, Water-Na$^+$, and Water-Cl$^-$ are shown in Table I. The other correlations are omitted because they are much smaller, as clearly seen in Fig. 1. Then, the Van Hove function, which is calculated by the double Fourier transformation of $S(Q,E)$, can be expressed as the combination of the pseudopartial Van Hove functions, $G'_{\alpha\beta}(R,t)$, as follows:

$$G(R,t) - 1 = \sum_{\alpha\beta} \overline{w_{\alpha\beta}} [G'_{\alpha\beta}(R,t) - 1]. \quad (7)$$

Note that $G'_{\alpha\beta}(R,t)$ is slightly different from the partial Van Hove function, $G_{\alpha\beta}(R,t)$, defined in Eq. (3). Even though this is a rough estimation, it is useful enough for estimating the amount of contribution from each correlation to the calculated Van Hove function.

III. RESULTS AND DISCUSSION

A. Van Hove function of salt water

Figure 2 shows the Van Hove functions of pure water and the aqueous solutions of NaCl. As shown in the previous study, the shift in the first and second peak is clearly seen for the pure water; the first-neighbor peak position moves

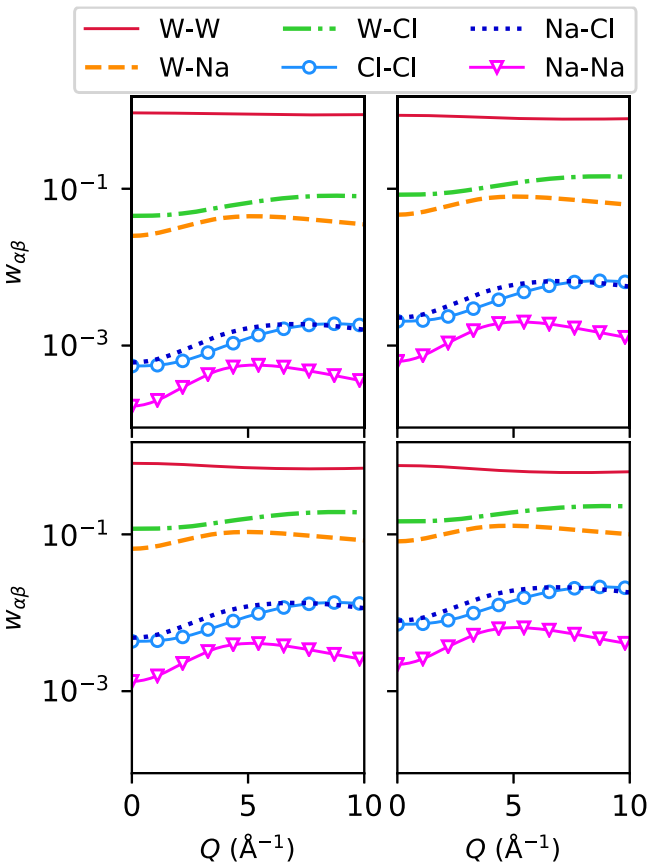

FIG. 1. Comparison of $w_{\alpha\beta}(Q)$: m = (upper left) 0.75, (upper right) 1.5, (lower left) 2.26, and (lower right) 3.0 mol/kg. W stands for water molecule.

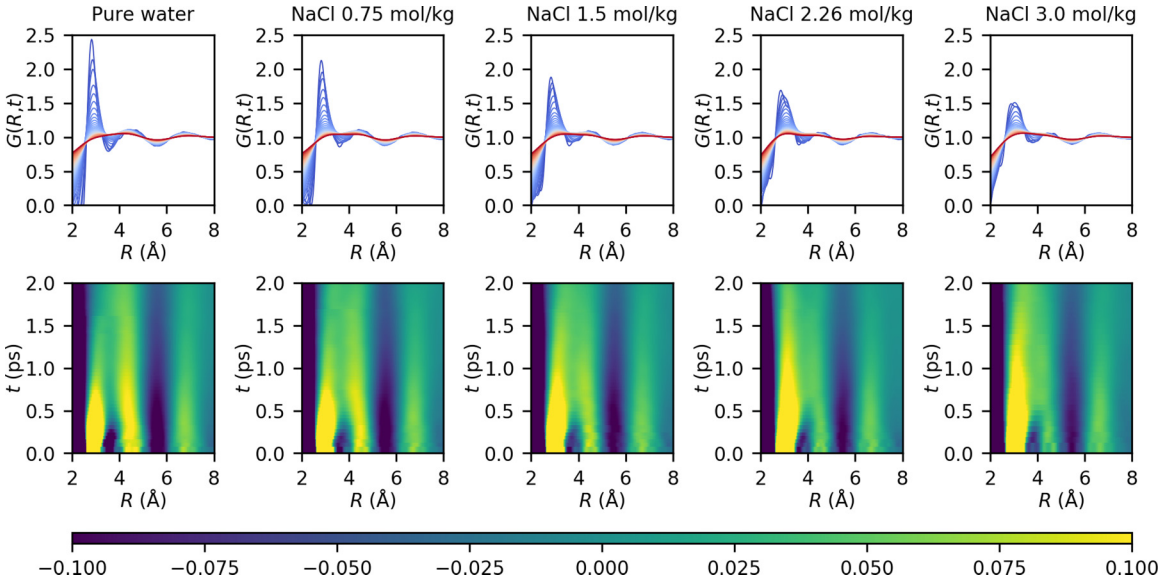

FIG. 2. The Van Hove function of a NaCl aqueous solution. Top: One-dimensional slice of the Van Hove functions, $G(R, t)$, at $0 < t < 2$ ps. Middle: Intensity map of $G(R, t) - 1$, the color scale of which is shown in the bottom. Left to right: $m = 0$ (pure water), 0.75, 1.5, 2.26, and 3.0 mol/kg.

with time toward a higher R and the second peak position moves toward a lower R. This is in sharp contrast to the case of metallic liquid, for which the peak positions remain mostly unchanged [36,50]. The shift indicates that the first and second neighbors are dynamically coupled due to the existence of a hydrogen bond and the small coordination number [36,37].

The addition of salt induces the changes in the shape of Van Hove function profiles. Regarding the snapshot structure ($t = 0$), the amplitude of the correlation functions decreases with the increase in the salt concentration, as is expected from the previous neutron scattering studies [20]. These changes may be interpreted as the result of phase mismatching in the oscillation of the Van Hove function: the positions of the individual radial distribution functions for O-O, O-Na^+, and O-Cl^- are estimated to be around 2.8 Å, 2.3 Å, and 3.2 Å, respectively [21]. In the current measurement, all of these contribute to the Van Hove function. These values of ionic radii are close to each other, but are sufficiently different so that the scattering from each component is canceled out or smeared due to the phase mismatch on the oscillation. An enlarged view at around the first-neighbor peak (Fig. 3) indicates the emergence of the correlation between water and Cl^- around the distance which corresponds to the sum of the ionic radii of O^{2-} and Cl^-.

At a longer timescale ($t > 0.5$ ps), the addition of salt induces a qualitative change at the first- and the second-neighbor peaks. The addition of salt makes the decay time of the first-neighbor peak longer, as is discussed in detail in the next section, whereas the amplitude of the second-neighbor peak is drastically decreased by salt. Therefore, the first-neighbor correlation is dominant in the NaCl aqueous solution at $t < 1.0$ ps. This is in stark contrast to the case of pure water, where the second-neighbor peak at around $R = 4.2$ Å is dominant after the first-neighbor peak at around $R = 2.8$ Å fully decays at around $t = 1$–1.5 ps [37].

Because of the intrinsic broad width of the correlation profiles, it is difficult to separate the profiles into those of each individual oxygen-ion correlation *a priori*. Therefore, we first discuss the overall correlated motions between neighboring water molecules and salt ions. Then, we discuss the contribution of oxygen-ion correlations by focusing on the variation in the Van Hove function induced by salt ions.

B. Temporal evolution of the first-neighbor peak

The decaying behavior of the first-neighbor peak, $R = R_1$, is directly related to the correlated motions between neighboring molecules, thereby largely determining the transport phenomena such as viscosity, as shown in the previous studies [37]. We find that the addition of salt induces the changes in the decaying behavior of the peak area, $A_1(t)$, at the first-neighbor peak, as shown in Fig. 4. Here, the peak area is defined as $A_1(t) = \int_{R_1'}^{R_1''} [G(R, t) - 1] dR$, where R_1' and R_1'' are defined as shown in Fig. 3. To estimate the uncertainties, the upper bound R_1'' was changed within the gray-shaded region in Fig. 3.

Pure water shows a two-step relaxation behavior, as observed in the previous study [37]. The two-step decay is also observed for the samples of the aqueous solution of NaCl, but with the addition of salt, the amplitude of the first step decay is decreased (see the inset of Fig. 4), while that of the second-step decay is increased except for the highest concentration sample ($m = 3.0$ mol/kg), which shows a decay similar to that of the 2.26 mol/kg sample. The choice of R_1'' is somewhat arbitrary, but the uncertainties that were estimated by changing R_1'' hardly influence the following discussion.

This two-step decaying behavior is fitted by using the summation of two compressed exponential functions, $A_1(t) = a_1 \exp[-(t/\tau_1)^{p_1}] + a_2 \exp[-(t/\tau_2)^{p_2}]$, with $\tau_1 < \tau_2$. The result of the fitting and $A_1(0)$ are shown in Fig. 5. The addition

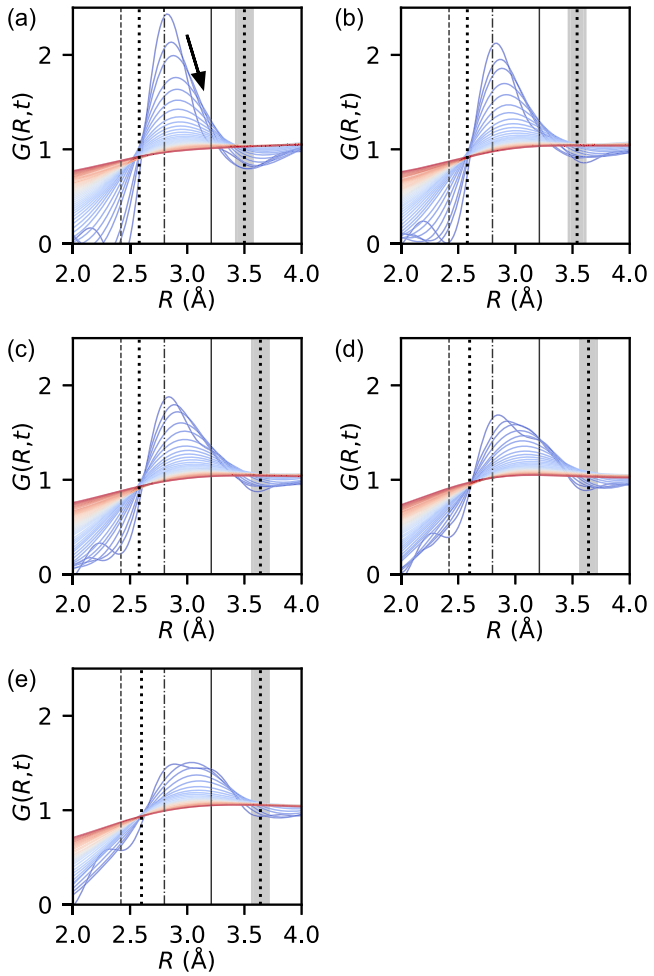

FIG. 3. Enlarged view of Van Hove functions at around the first-neighbor correlation peak, $R \sim 2.9$ Å: (a) pure water, (b) $m = 0.75$ mol/kg, (c) 1.5 mol/kg, (d) 2.26 mol/kg, and (e) 3.0 mol/kg. The solid lines at $R = 3.21$ Å show the $R_{O^{2-}} + R_{Cl^-}$. The dashed line at $R = 2.42$ Å shows the $R_{O^{2-}} + R_{Na^+}$. The dash-dotted line at $R = 2.8$Å shows the $R_{O^{2-}} + R_{O^{2-}}$. The range between the dotted lines (R_1' and R_1'') was used to calculate the area, $A(t)$, of the first neighbor. The upper limit of this range is changed within the gray-shaded area to estimate the uncertainties.

of salt decreases a_1 and increases a_2, while $A_1(0)$ is decreased. The decrease in $A_1(0)$ indicates a reduction in the apparent coordination number at R_1. The exponent of the second step decay, p_2, for the pure water sample is similar to those observed in the previous study [37] and is much higher than that for the aqueous salt solutions.

It has been assumed that the salt influences the dynamics of the first hydration layer or some extended region beyond the first hydration layer [10,11]. It is then natural to assume that the correlated dynamics of water molecules that are not close to the ions is identical to that in pure water, while the presence of ions may influence the motions of surrounding water molecules. The amount of volume in which the ions affect the dynamics of water will be proportional to the molality up to m_c at which the hydration layers around the ions start to overlap. With this assumption, the decaying behavior of 0.75 and 1.5 mol/kg is expressed as the linear combination

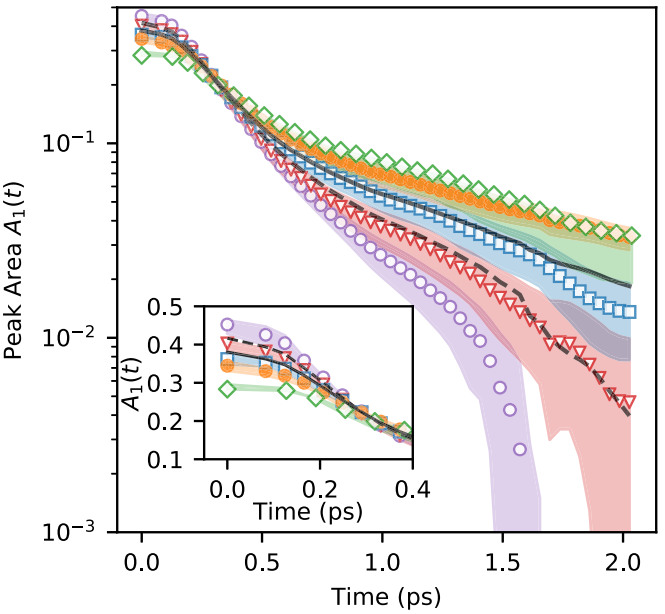

FIG. 4. Temporal changes in the area of the first-neighbor peak, $A_1(t)$, and the enlarged view (inset): (open circles) pure water, (triangles) $m = 0.75$ mol/kg, (squares) 1.5 mol/kg, (closed circles) 2.26 mol/kg, and (diamonds) 3.0 mol/kg. The shaded areas represent uncertainties of each dataset. The solid and dashed lines represent the linear combination of time evolution for $m = 0$ and 2.26 mol/kg (see the main text).

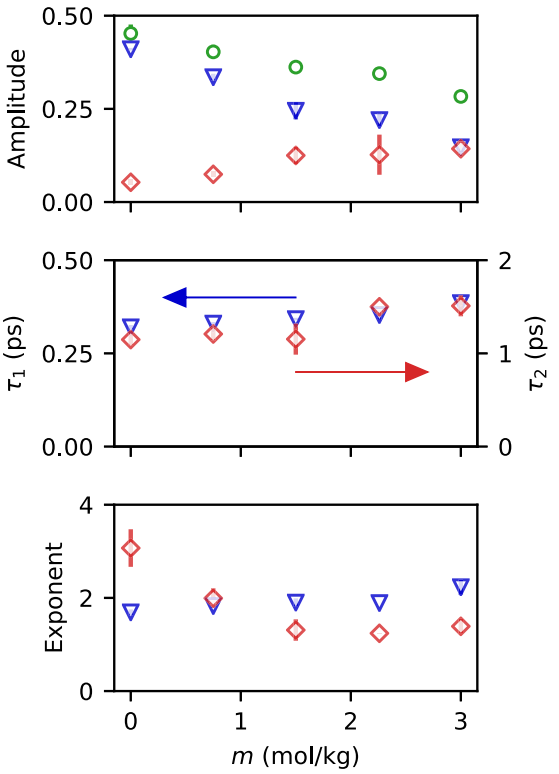

FIG. 5. Fitting results of the first-neighbor decay. (Triangles) a_1, τ_1, p_1, (diamonds) a_2, τ_2, p_2, and (circles) $A_1(0)$. The error bar is estimated by the standard deviation of the fitting.

of the decaying behaviors of pure water and NaCl solutions in a higher concentration:

$$A_1(t,m) = \frac{2.26 - \frac{m}{\text{mol/kg}}}{2.26} A_1(t, m=0) + \frac{\frac{m}{\text{mol/kg}}}{2.26} A_1(t, m = 2.26\,\text{mol/kg}). \quad (8)$$

Here we use $A_1(t, m = 2.26\,\text{mol/kg})$ instead of $A_1(t, m = 3.0\,\text{mol/kg})$, simply because apparently the region that is influenced by the salt is saturated at concentrations higher than 2.26 mol/kg. The result of the linear combination for $m = 0.75$ (dashed line) and 1.5 mol/kg (solid line) is shown in Fig. 4; their agreement with the $A_1(t, m = 0)$ and $A_1(t, m = 1.5\,\text{mol/kg})$ is good enough to conclude that their decay behavior can be expressed as the linear combination of that of the bulk water and the hydration layers. The fact that all the decay curves intersect at $t = 0.28$ ps supports that the spectra are decomposed into the linear combination.

C. Correlation functions between water and ions

The Van Hove function is made of the contributions from the water-water correlations and the water-ion correlations because the ion-ion contribution is negligible at these salt concentrations. The discussion above promotes us to assume that these contributions are independent of the salt concentration, at least in the zeroth order. Then the Van Hove function, $G(R,t)$, may be expressed as the linear combination of the Van Hove function of pure water, $G_{\text{pure}}(R,t)$, and the pseudopartial Van Hove functions for water and ions as follows:

$$G(R,t) - 1 \approx \overline{w_{\text{w-w}}}[G_{\text{pure}}(R,t) - 1] + \overline{w_{\text{w-Cl}}}[G'_{\text{w-Cl}}(R,t) - 1] + \overline{w_{\text{w-Na}}}[G'_{\text{w-Na}}(R,t) - 1]. \quad (9)$$

Here, the weighting factors $\overline{w_{\alpha\beta}}$ are given in Table I and w stands for a water molecule. Because $\overline{w_{\text{w-Na}}}/\overline{w_{\text{w-Cl}}} \sim 0.58$, we may focus on the water-Cl correlation and express the temporal correlations between water and ions by the following:

$$G'(R,t) = \frac{G_m(R,t) - 1 - \overline{w_{\text{w-w}}}[G_{\text{pure}}(R,t) - 1]}{\overline{w_{\text{w-Cl}}}} \approx [G'_{\text{w-Cl}}(R,t) - 1] + \frac{\overline{w_{\text{w-Na}}}}{\overline{w_{\text{w-Cl}}}}[G'_{\text{w-Na}}(R,t) - 1]. \quad (10)$$

The time evolution and its intensity map for each molality are shown in Fig. 6. At a short time ($t < 0.3$ ps), positive correlation peaks are observed at a distance corresponding to $R = R_{O^{2-}} + R_{Na^+}$ (= 2.42 Å) and $R = R_{O^{2-}} + R_{Cl^-}$ (= 3.21 Å), while a negative correlation peak is observed at $R = R_{O^{2-}} + R_{O^{2-}}$ (=2.8). The positive correlations represent the correlation between a water molecule and a cation or an anion, respectively, while the negative correlation underscores that there is anticorrelation between water and ions. The peak values of the negative correlation at $R = R_{O^{2-}} + R_{O^{2-}}$ are strongly negative, around -2.5 at $t = 0$, indicating that the correlation between water molecules is perturbed in the hydration shell. It is possible that the local water-water coordination is reduced in the hydration shell, thereby leading to the significantly negative peak values. This interpretation

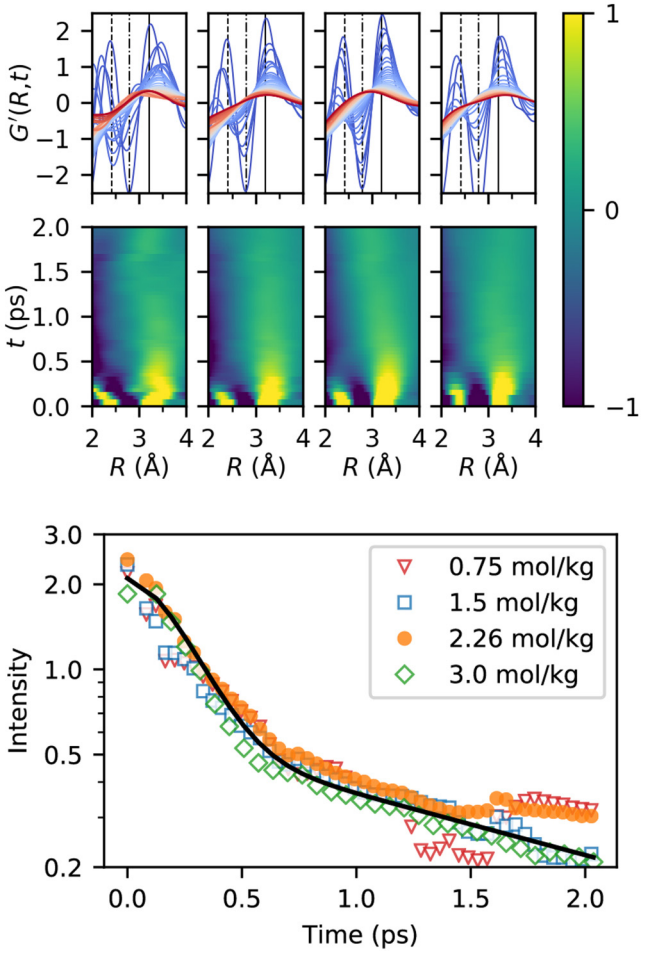

FIG. 6. One-dimensional profiles of $G'(R,t)$ at $0 < t < 2$ ps and (middle) their intensity maps. Their color scale is shown in the right. The molality of the sample is 0.75, 1.5, 2.26, 3.0 mol/kg, from the left to the right. The solid lines, dashed lines, and the dash-dotted lines in the top figures represent $R = 3.21$ Å$(R_{O^{2-}} + R_{Cl^-})$, $R = 2.42$ Å$(R_{O^{2-}} + R_{Na^+})$, and $R = 2.8$ Å$(R_{O^{2-}} + R_{O^{2-}})$, respectively. Bottom: Time evolution of the peak height at around $R = 3.21$ Å. The solid line shows the result of fitting using two (compressed) exponential functions (see main text).

is consistent with the result of a neutron diffraction study [13], which concluded that the first peak height in the pair-distribution function for water-water correlations is reduced by the addition of NaCl.

The panels in Fig. 6 (top and middle) are similar to each other, underscoring our assumption that the decaying behaviors of water-Na^+ and water-Cl^- correlations are independent of salt concentration, although quantitative discussion is limited due to a contamination of termination errors in the Van Hove functions at a short time, particularly at $t < 0.2$ ps, and the approximation used for the calculation. The decaying behavior of the peak height at around $R = R_{O^{2-}} + R_{Cl^-}$ (water-Cl^- correlations) is approximated by a two-step relaxation, $I(t) = 1.5\exp[-(t/0.32\,\text{ps})^{1.7}] + 0.6\exp(-t/2.0\,\text{ps})$, as shown by the solid line in Fig. 7 (bottom). The first term is almost identical to that of pure water ($\tau_1 = 0.32$ ps), except for its amplitude, indicating that

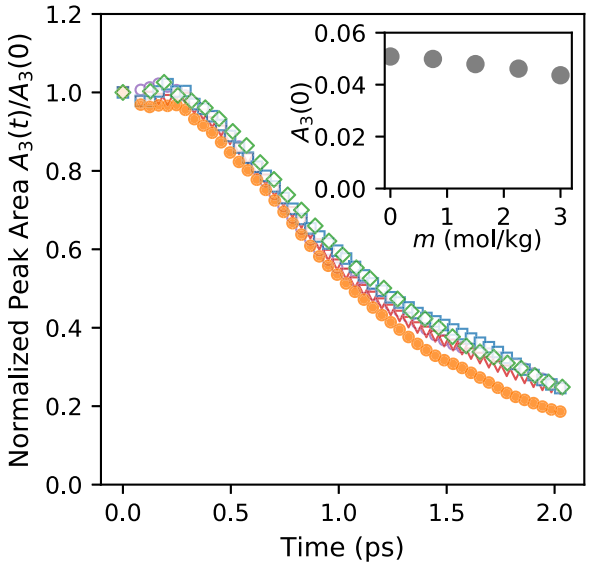

FIG. 7. Normalized temporal changes in the area of the third peak, $A_3(t)/A_3(0)$, around $R = 6.8$ Å; (open circles) pure water, (triangles) $m = 0.75$ mol/kg, (squares) 1.5 mol/kg, (closed circles) 2.26 mol/kg, and (diamonds) 3.0 mol/kg. Inset: Dependence of $A_3(0)$ on the molality.

the decaying at a short timescale ($t < 0.3$ ps) corresponds to a ballistic, caged motion, as was observed for the pure water. The second term represents the presence of a slow decay in the correlation between water and Cl^-, which dominates the decaying behavior at the first neighbor in Fig. 4. The correlated motions between a water molecule and a Cl^- ion are slower than that of water-water correlations with a decaying time ~2 ps, and it is most likely that this correlation is the principal mechanism of the slowing down shown in Fig. 4. A thorough research using other types of ions would show us how the water-ion correlation depends on the nature of ions.

D. Correlations at a long distance

In contrast to the first- and second-neighbor peaks, the third-neighbor peak at around $R = 6.8$ Å is hardly dependent on the addition of salt. Figure 7 shows the temporal evolution of the area, $A_3(t)$, at the third peak, which is normalized by $A_3(0)$. The normalized values collapse into a single decaying curve, even though $A_3(0)$ gently decreases with the addition of salt. This indicates that the dynamics of the NaCl aqueous solution is approximately the same at long distances, regardless of the molality, which has been discussed in terms of a snapshot structure of the aqueous salt solution [34], and qualitatively agrees with the concept of "sticky ions" [51].

The values of the normalized amplitude remain almost constant for $t < 0.3$ ps, indicating that the first-step decay at the first neighbor in the averaged Van Hove functions is absent for the third peak. As was discussed elsewhere [50], the higher-order peaks of the PDF and the Van Hove function do not represent a single atom-atom distance, but the density correlations among the aggregate of many atoms. Therefore, the decay time of the higher-order peaks does not correspond to the microscopic timescale. Indeed, the dynamics at the third-neighbor peak is barely dependent on the salt concentration.

IV. CONCLUDING REMARKS

Usually the dynamics of liquid is discussed in terms of the dynamic structure function, $S(Q, E)$, or the intermediate scattering function, $F(Q, t)$. In particular, the decay time of the first peak ($Q = Q_1$) of $F(Q, t)$ is called the α-relaxation time and has been widely used to discuss the dynamics of liquid. However, the first peak of $F(Q, t)$ includes all the contributions from the long-range correlations and is dominated by the geometrical factor in many cases rather than the microscopic dynamics [50]. This point underscores the importance of discussing the liquid dynamics in terms of the Van Hove function $G(R, t)$. The effect of salt on the dynamics, within the hydration layers in particular, needs to be examined using the correlation function in real space, not in reciprocal space.

We showed that a real-space visualization of correlated molecular/ionic dynamics in a picosecond timescale and sub-nm scale using the Van Hove function can be applied to aqueous solutions of sodium chloride to determine the effect of salt addition to the local correlated dynamics of water. The results depict how salt ions alter the local correlated molecular motions through the interaction between water and salt ions. The effect is local, not long range, and is limited to within the hydration cells, which is comparable to what is observed for the reorientation dynamics by optical spectroscopy. Because of the importance of salt water to life and other activities, elucidating the effect of salt addition to water at the microscopic level is crucial in advancing the life sciences. The present result represents a major step forward to understanding the transport properties, such as viscosity and conductivity, of complex aqueous solutions based on the molecular-level correlated dynamics.

The U.S. Department of Energy will provide public access to these results of federally sponsored research in accordance with the U.S. DOE Public Access Plan [52] .

ACKNOWLEDGMENTS

This work was sponsored by the Laboratory Directed Research and Development Program of Oak Ridge National Laboratory, which is managed by UT-Battelle, LLC, under Contract No. DE-AC05-00OR22725 for the U.S. Department of Energy. IXS experiments at BL43LXU, SPring-8 were conducted under the approval of RIKEN (Proposals No. 20160102, No. 20170075, and No. 20180069). This research used resources of the Advanced Photon Source, a U.S. Department of Energy (DOE) Office of Science User Facility operated for the U.S. DOE Office of Science by Argonne National Laboratory under Contract No. DE-AC02-06CH11357. High-energy x-ray diffraction measurement at 6-ID-D, APS, was conducted with the help of Dr. D. Robinson.

[1] D. Laage, T. Elsaesser, and J. T. Hynes, Water dynamics in the hydration shells of biomolecules, Chem. Rev. **117**, 10694 (2017).

[2] E. Brini, C. J. Fennell, M. Fernández-Serra, B. Hribar-Lee, M. Lukšič, and K. A. Dill, How water's properties are encoded in its molecular structure and energies, Chem. Rev. **117**, 12385 (2017).

[3] G. Jones and M. Dole, The viscosity of aqueous solutions of strong electrolytes with special reference to barium chloride, J. Am. Chem. Soc. **51**, 2950 (1929).

[4] H. D. B. Jenkins and Y. Marcus, Viscosity b-coefficients of ions in solution, Chem. Rev. **95**, 2695 (1995).

[5] S. Ansell, A. C. Barnes, P. E. Mason, G. W. Neilson, and S. Ramos, X-ray and neutron scattering studies of the hydration structure of alkali ions in concentrated aqueous solutions, Biophys. Chem. **124**, 171 (2006).

[6] Y. Chen, H. I. Okur, N. Gomopoulos, C. Macias-Romero, P. S. Cremer, P. B. Petersen, G. Tocci, D. M. Wilkins, C. Liang, M. Ceriotti, and S. Roke, Electrolytes induce long-range orientational order and free energy changes in the H-bond network of bulk water, Sci. Adv. **2**, e1501891 (2016).

[7] Y. Chen, H. I. Okur, C. Liang, and S. Roke, Orientational ordering of water in extended hydration shells of cations is ion-specific and is correlated directly with viscosity and hydration free energy, Phys. Chem. Chem. Phys. **19**, 24678 (2017).

[8] A. Shalit, S. Ahmed, J. Savolainen, and P. Hamm, Terahertz echoes reveal the inhomogeneity of aqueous salt solutions, Nat. Chem. **9**, 273 (2017).

[9] H. J. Bakker, Structural dynamics of aqueous salt solutions, Chem. Rev. **108**, 1456 (2008).

[10] K. J. Tielrooij, N. Garcia-Araez, M. Bonn, and H. J. Bakker, Cooperativity in ion hydration, Science **328**, 1006 (2010).

[11] M. F. Kropman and H. J. Bakker, Dynamics of water molecules in aqueous solvation shells, Science **291**, 2118 (2001).

[12] R. Buchner, G. T. Hefter, and P. M. May, Dielectric relaxation of aqueous NaCl solutions, J. Phys. Chem. A **103**, 1 (1999).

[13] R. Mancinelli, A. Botti, F. Bruni, M. A. Ricci, and A. K. Soper, Perturbation of water structure due to monovalent ions in solution, Phys. Chem. Chem. Phys. **9**, 2959 (2007).

[14] I. Waluyo, C. Huang, D. Nordlund, U. Bergmann, T. M. Weiss, L. G. M. Pettersson, and A. Nilsson, The structure of water in the hydration shell of cations from x-ray Raman and small angle x-ray scattering measurements, J. Chem. Phys. **134**, 064513 (2011).

[15] H. Ohtaki and T. Radnai, Structure and dynamics of hydrated ions, Chem. Rev. **93**, 1157 (1993).

[16] T. Corridoni, R. Mancinelli, M. A. Ricci, and F. Bruni, Viscosity of aqueous solutions and local microscopic structure, J. Phys. Chem. B **115**, 14008 (2011).

[17] M. Andreev, J. J. de Pablo, A. Chremos, and J. F. Douglas, Influence of ion solvation on the properties of electrolyte solutions, J. Phys. Chem. B **122**, 4029 (2018).

[18] J. D. Bernal and R. H. Fowler, A theory of water and ionic solution, with particular reference to hydrogen and hydroxyl ions, J. Chem. Phys. **1**, 515 (1933).

[19] Y. Marcus, Effect of ions on the structure of water: Structure making and breaking, Chem. Rev. **109**, 1346 (2009).

[20] G. W. Neilson, P. E. Mason, S. Ramos, and D. Sullivan, Neutron and x-ray scattering studies of hydration in aqueous solutions, Philos. Trans. R. Soc. A: Math. Phys. Eng. Sci. **359**, 1575 (2001).

[21] R. Mancinelli, A. Botti, F. Bruni, M. A. Ricci, and A. K. Soper, Hydration of sodium, potassium, and chloride ions in solution and the concept of structure maker/breaker, J. Phys. Chem. B **111**, 13570 (2007).

[22] S. Bouazizi, S. Nasr, N. Jaîdane, and M.-C. Bellissent-Funel, Local order in aqueous NaCl solutions and pure water: X-ray scattering and molecular dynamics simulations study, J. Phys. Chem. B **110**, 23515 (2006).

[23] B. Hribar, N. T. Southall, V. Vlachy, and K. A. Dill, How ions affect the structure of water, J. Am. Chem. Soc. **124**, 12302 (2002).

[24] R. Leberman and A. K. Soper, Effect of high-salt concentrations on water-structure, Nature (London) **378**, 364 (1995).

[25] A. W. Omta, M. F. Kropman, S. Woutersen, and H. J. Bakker, Negligible effect of ions on the hydrogen-bond structure in liquid water, Science **301**, 347 (2003).

[26] J. Duboisset and P.-F. Brevet, Salt-Induced Long-To-Short Range Orientational Transition in Water, Phys. Rev. Lett. **120**, 263001 (2018).

[27] S. Funkner, G. Niehues, D. A. Schmidt, M. Heyden, G. Schwaab, K. M. Callahan, D. J. Tobias, and M. Havenith, Watching the low-frequency motions in aqueous salt solutions: The terahertz vibrational signatures of hydrated ions, J. Am. Chem. Soc. **134**, 1030 (2011).

[28] F. Perakis, L. De Marco, A. Shalit, F. Tang, Z. R. Kann, T. D. Kühne, R. Torre, M. Bonn, and Y. Nagata, Vibrational spectroscopy and dynamics of water, Chem. Rev. **116**, 7590 (2016).

[29] A. P. Gaiduk and G. Galli, Local and global effects of dissolved sodium chloride on the structure of water, J. Phys. Chem. Lett. **8**, 1496 (2017).

[30] G. Stirnemann, E. Wernersson, P. Jungwirth, and D. Laage, Mechanisms of acceleration and retardation of water dynamics by ions, J. Am. Chem. Soc. **135**, 11824 (2013).

[31] S. Chowdhuri and A. Chandra, Molecular dynamics simulations of aqueous NaCl and KCl solutions: Effects of ion concentration on the single-particle, pair, and collective dynamical properties of ions and water molecules, J. Chem. Phys. **115**, 3732 (2001).

[32] Y. Ding, A. A. Hassanali, and M. Parrinello, Anomalous water diffusion in salt solutions, Proc. Nat. Acad. Sci. USA **111**, 3310 (2014).

[33] J. S. Kim, Z. Wu, A. R. Morrow, A. Yethiraj, and A. Yethiraj, Self-diffusion and viscosity in electrolyte solutions, J. Phys. Chem. B **116**, 12007 (2012).

[34] M. Andreev, A. Chremos, J. de Pablo, and J. F. Douglas, Coarse-grained model of the dynamics of electrolyte solutions, J. Phys. Chem. B **121**, 8195 (2017).

[35] T. Iwashita, D. M. Nicholson, and T. Egami, Elementary Excitations and Crossover Phenomenon in Liquids, Phys. Rev. Lett. **110**, 205504 (2013).

[36] T. Iwashita, B. Wu, W.-R. Chen, S. Tsutsui, A. Q. R. Baron, and T. Egami, Seeing real-space dynamics of liquid water through inelastic x-ray scattering, Sci. Adv. **3**, e1603079 (2017).

[37] Y. Shinohara, W. Dmowski, T. Iwashita, B. Wu, D. Ishikawa, A. Q. R. Baron, and T. Egami, Viscosity and real-space molecular motion of water: Observation with inelastic x-ray scattering, Phys. Rev. E **98**, 022604 (2018).

[38] M. E. Blodgett, T. Egami, Z. Nussinov, and K. F. Kelton, Proposal for universality in the viscosity of metallic liquids, Sci. Rep. **5**, 13837 (2015).

[39] T. Egami, Elementary excitation and energy landscape in simple liquids, Mod. Phys. Lett. B **28**, 1430006 (2014).

[40] L. Van Hove, Correlations in space and time and born approximation scattering in systems of interacting particles, Phys. Rev. **95**, 249 (1954).

[41] A. Q. R. Baron, High-resolution inelastic x-ray scattering I: Context, spectrometers, samples, and superconductors, in *Synchrotron Light Sources and Free Electron Lasers Accelerator Physics*, edited by E. Jaeschke, S. Khan, J. R. Schneider, and J. B. Hastings (Springer International, Cham, Switzerland, 2016), pp. 1643–1719.

[42] A. Q. R. Baron, High-resolution inelastic x-ray scattering II: Scattering theory, harmonic phonons, and calculations, in *Synchrotron Light Sources and Free Electron Lasers Accelerator Physics*, edited by E. Jaeschke, S. Khan, J. R. Schneider, and J. B. Hastings (Springer International, Cham, Switzerland, 2016), pp. 1721–1757.

[43] Y. Kawakita, T. Kikuchi, Y. Inamura, S. Tahara, K. Maruyama, T. Hanashima, M. Nakamura, R. Kiyanagi, Y. Yamauchi, K. Chiba, S. Ohira-Kawamura, Y. Sakaguchi, H. Shimakura, R. Takahashi, and K. Nakajima, Anomaly of structural relaxation in complex liquid metal of bismuth - dynamic correlation function of coherent quasi-elastic neutron scattering, Physica B **551**, 291 (2018).

[44] R. Ashcraft, Z. Wang, D. L. Abernathy, T. Egami, and K. F. Kelton, Experimental measurements of the temperature-dependent Van Hove function in a $Zr_{80}Pt_{20}$ liquid - Confirmation of a structural origin for the dynamics at high temperature, arXiv:1810.02351.

[45] A. Q. R. Baron, Status of the RIKEN Quantum NanoDynamics Beamline (BL43LXU): The Next Generation for Inelastic X-ray Scattering, SPring-8 Inf. Newsl. **15**, 14 (2010).

[46] A. P. Hammersley, Fit2D: An Introduction and Overview, Report No. ESRF97HA02T (ESRF, France, 1997).

[47] T. Egami and S. J. L. Billinge, *Underneath the Bragg Peaks: Structural Analysis of Complex Materials* (Pergamon, Amsterdam, 2012).

[48] D. Waasmaier and A. Kirfel, New analytical scattering-factor functions for free atoms and ions, Acta Crystallogr. Sec. A **51**, 416 (1995).

[49] J. Wang, A. N. Tripathi, and V. H. Smith, Jr., Chemical binding and electron correlation effects in x-ray and high energy electron scattering, J. Chem. Phys. **101**, 4842 (1994).

[50] B. Wu, T. Iwashita, and T. Egami, Atomic Dynamics in Simple Liquid: De Gennes Narrowing Revisited, Phys. Rev. Lett. **120**, 135502 (2018).

[51] K. D. Collins, Sticky ions in biological systems, Proc. Natl. Acad. Sci. **92**, 5553 (1995).

[52] See http://energy.gov/downloads/doe-public-access-plan (unpublished).